Article

Development of an RHEB-Targeting Peptide To Inhibit mTORC1 Kinase Activity

Raef Shams, Yoshihiro Ito, and Hideyuki Miyatake*

Read Online

ACCESS | Metrics & More | Article Recommendations | Supporting Information

ABSTRACT: In cancer, the mechanistic/mammalian target of rapamycin complex-1 (mTORC1) is hyperactivated to promote survival under adverse conditions. The kinase activity of mTORC1 is activated by small-GTPase RHEB-GTP. Therefore, a new modality to inhibit mTORC1 activity has emerged, through intercepting RHEB. However, due to the relatively large contact area involved in the interaction between RHEB and mTORC1, facilitating this inhibition through small molecules has been challenging. Here, we report the development of a peptide that can inhibit the RHEB−mTORC1 interaction. The peptide, **P1_WT**, was designed based on the α-helix (aa 101−115) of the N-heat domain of mTOR to interact with switch II of RHEB. **P1_WT** bound to RHEB (K_D = 0.14 μM) and inhibited RHEB-mTOR$^{N\text{-heat}}$ interaction (IC_{50} = 0.33 μM) in vitro. Consequently, P1_WT inhibited mTORC1 activity at a sub-micromolar level ($IC_{50} \sim 0.3$ μM). **P1_WT** was predicted to be cell-permeable due to the rich content of arginine (23%), enhancing the intracellular translocation. These results show that **P1_WT** is a potential compound to further develop inhibitors for mTORC1 by intercepting RHEB from mTORC1.
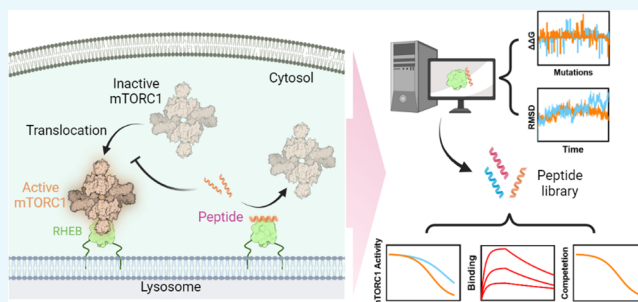
INTRODUCTION

The mechanistic/mammalian target of rapamycin complex 1 (mTORC1) is a serine/threonine protein kinase to regulate cell growth and proliferation.[1,2] mTORC1 consists of multiple components: the mTOR kinase unit, mammalian lethal with SEC13 protein 8 (mLST8), regulatory-associated protein of mTOR (RAPTOR), DEP domain-containing mTOR-interacting protein (DEPTOR), and the 40-kDa proline-rich AKT substrate (PRAS40).[2,3] These components work together to recruit and phosphorylate substrate proteins downstream the signal pathways such as the eukaryotic translation initiation factor 4E-binding protein (4E-BP1) and ribosomal protein S6 kinase 1 (S6K1).[3,4] Conversely, upstream the signaling pathway, the kinase activity of mTORC1 is modulated by growth factors, nutrients, and energy transfer to manage protein, lipid, and nucleotide synthesis.[5,6] These upstream signals are shown to control the activation process by coupling mTORC1 with the Ras homolog enriched in brain (RHEB) protein on the lysosomal surface.[3,7]

RHEB-GTPase is a small G-protein ($\sim$20 kDa) that is farnesylated to the lysosome membrane.[8] The GTPase activity of RHEB is stimulated by the tuberous sclerosis complex 1/2 (TSC1/2), the upstream negative regulator of mTORC1.[1,8] Thus, RHEB activates mTORC1 only when it is charged with GTP but not GDP.[3] Recently, structural studies have elucidated the activation mechanism of mTORC1 by the RHEB-GTP complex to allosterically bind to the constituted site formed by the N-heat, M-heat, and FAT domains of

mTOR. Upon binding, conformational changes over a wide area of the kinase domain of mTOR occur to receive ATP in the active site for catalysis.[3] On the lysosome surface, mTORC1 activation is cooperatively modulated via two in-parallel pathways; the first is the activation of RHEB by the TSC1/2 complex to enhance RHEB charging with GTP.[7] This pathway is controlled by growth factors, including the insulin-like growth factor (IGF), through IGF/PI3K/AKT pathways, which negatively or positively control TSC complexation.[1,5,9] The second pathway involves the translocation of mTORC1 onto the lysosome surface to form a complex with the RHEB-GTP. This translocation is regulated via the capturing process of the mTORC1 subunit, RAPTOR, by the Rags/Ragulator complex on the lysosome surface according to amino acid levels.[7,10,11]

To facilitate RHEB binding to the M-heat, FAT, and N-heat domains of mTOR, the switch I and II regions of RHEB should be conformationally changed by the GTP binding.[3] The switch I is destabilized upon the catalysis of GTP, which enables GDP/GTP nucleotide exchange. In contrast, the
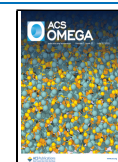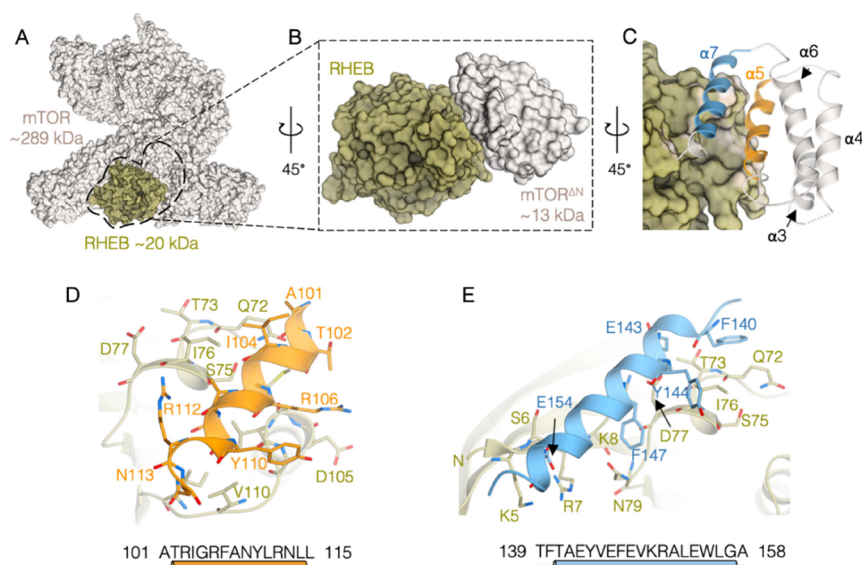
Figure 1. Structure-based design of RHEB-targeting peptides. (A) Molecular structure of monomeric mTORC1 to illustrate the mode of RHEB binding with mTOR (PDB ID: 6BCU). Raptor and mLST8 were omitted for clarity. (B and C) Close-up view of RHEB binding with the mTOR$^{\Delta N}$ domain (aa 60−167), showing α3, α4, α5, α6, and α7 helices of mTOR colored as indicated in (C). (D and E) Close-up of RHEB binding with α5-helix (D; aa 101−115) and α7-helix (E; aa 139−158) of mTOR, showing the residues involved in binding. Sequences and secondary structures are shown (helices = cylinders).
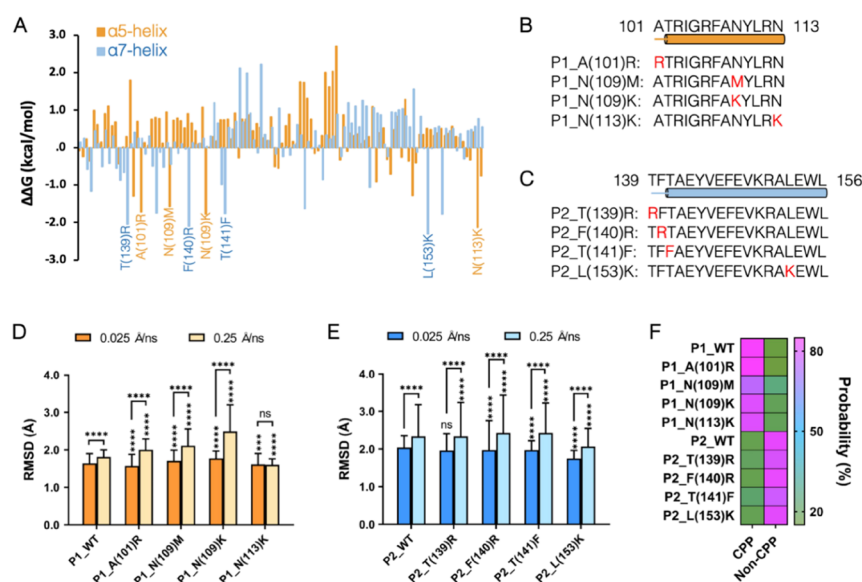
Figure 2. In silico selection of RHEB-targeting peptide. (A) In silico point mutagenesis of the interactive α5 and α7 helices of the mTOR$^{\Delta N}$ domain (aa 60−167) at the mTOR−RHEB interface extracted from the mTORC1 structure (PDB ID: 6BCU). The free energy was calculated using the following equation: $\Delta\Delta G_{bind} = \Delta G_{mutant} - \Delta G_{WT}$, and the best results are indicated. (B and C) Wild type and the corresponding variant sequences of α5-helix (B; hereinafter named **P1**) and α7-helix (C; hereinafter named **P2**) showing the point-mutated residues in red color. (D and E) Steered molecular dynamics studies showing the deviation of P1 variants (D) and P2 variants (E) from the initial binding pose under two different pulling forces (0.025 and 0.25 Å/ns) represented by the root-mean square deviation (RMSD). The results represent the mean of the collected points along the simulation time ($n = 5000$) ± SD. Two-way ANOVA was used (****$P < 0.0001$; ns, $P > 0.05$) with Tukey's test correction. (F) Prediction of cell penetration probability of the indicated peptides using the MLCPP online tool (http://www.thegleelab.org/MLCPP/MLCPP.html). The results are indicated as a percentage of total probability. CPP, Cell-penetrating peptides; Non-CPP, Non Cell-penetrating peptides.

switch II remains stable during binding to govern mTORC1 activation.[8,12] Point mutation in the specific residues (aa 67−77) of switch II prohibits mTORC1 activation.[13] In addition, because RHEB is farnesylated to the lysosomal membrane by farnesyltransferases, the inhibitors of these enzymes impair the post-translational modification of RHEB, resulting in mTORC1 inhibition.[14,15] However, these inhibitors are nonspecific to the enzymes, which limits precise targeting to RHEB.[16,17] Recently, it was reported that a small-molecule inhibitor, NR1 (HY124793), specifically binds to the switch II region of RHEB, leading to the inhibition of mTORC1 activity with a micromolar level of half-maximal inhibitory concentration (IC_{50}).[8] This result suggests a new modality of
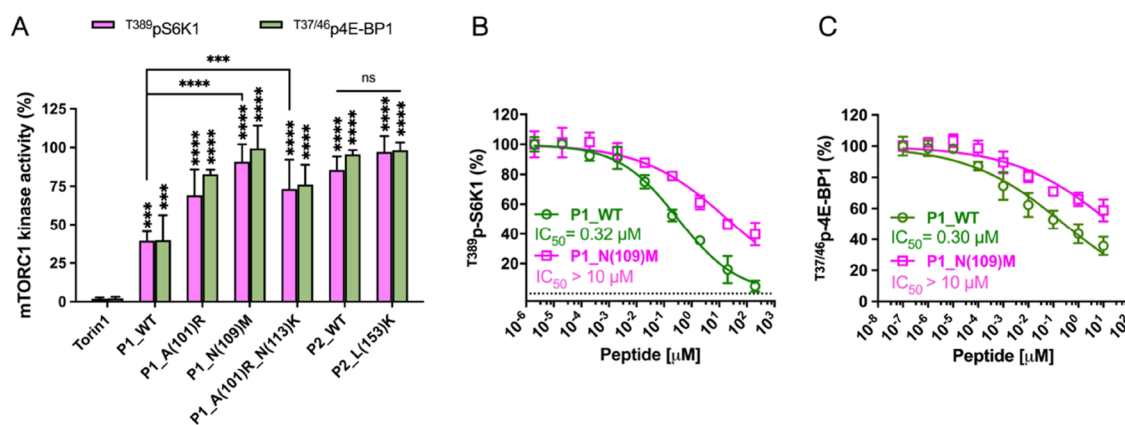
Figure 3. Inhibition of mTORC1 activity by RHEB-targeting peptides. (A) Screening of selected peptides for S6K1 and 4E-BP1 phosphorylation inhibition. HeLa cells were treated with a single dose (1 μM) of peptides or Torin1 for 3 h under starvation conditions and induced by 100 nM insulin for 30 min. The results represent the mean of two independent experiments as a percent of the controls ($n = 3$) $\pm$ SD. Two-way ANOVA was used (****$P < 0.0001$; ***$P < 0.001$; ns, $P > 0.05$) with Tukey's test correction. (B and C) Inhibition curves of ^{T389}p-S6K1 (B) and $^{T37/46}$p-4E-BP1 (C) of prestarved HeLa cells treated with increasing concentrations of **P1_WT** or **P1_N(109)M** peptides for 3 h and induced with 100 nM insulin for 30 min. The results are representative of two independent experiments as a percent of the controls ($n = 3$) $\pm$ SD. The half-maximal inhibitory concentrations (IC$_{50}$) are shown.

mTORC1 inhibition by interfering with protein−protein interaction (PPI).[8]

Targeting the PPI through small molecules is challenging due to the large interaction area. Therefore, the sizes of potential PPI inhibitors should be considered.[18] We used the structure-based drug design approach to develop peptide inhibitors to interfere with RHEB binding to mTORC1. Structural studies revealed that the N-heat domain of mTOR (mTOR$^{\Delta N}$; aa 60−167) interfaces RHEB with the α5- and α7-helices, wherein the α5-helix (aa 101−115) binds with the switch II region of RHEB (Figure 1).[3] Therefore, in this study, we report the development of a small peptide, **P1_WT**, that mimics the α5-helix (Figure 1D) with a predicted cell penetration property to interfere with RHEB-mTORC1 interaction, resulting in mTORC1 inhibition. We developed a strategy of in silico and in vitro methods to identify the proper peptide sequences with the aim of targeting RHEB with high affinity.[19,20]

RESULTS AND DISCUSSION

In Silico Development of RHEB-Binding Peptides. Previously, we studied the molecular interactions of RHEB with full-length mTOR and mTOR$^{\Delta N}$, yielding K_D values of ∼2.4 and 6.4 μM, respectively.[12] In the RHEB-mTOR$^{\Delta N}$ interface, α5- and α7-helices of mTOR$^{\Delta N}$ stabilize the mTORC1-RHEB complexation followed by the kinase activations.[3] The residues (aa 63−79) of RHEB in the switch II region lie between α5- and α7-helices, where α5 interacts with Q72, T73, S75, I76, and D77 residues of RHEB (Figure 1D), while α7 interacts with the same residues with the extension to bind with N79 and N-terminal resides (K5, S6, R7, and K8; Figure 1E).[3]

This structural information guided us in applying an in silico point-mutagenesis approach using ICM-Pro 3.9 software (Molsoft L.L.C., USA) to screen and mature the potential affinities of peptides for RHEB.[21] This was conducted by calculating the free binding energy ($\Delta\Delta G_{bind}$) for each residue of the peptide using the following equation:

$$\Delta\Delta G_{bind} = \Delta G_{mutant} - \Delta G_{WT}$$

where the free binding energy was calculated by subtracting the wild type of free energy (ΔG_{WT}) from the point-mutant free energy (ΔG_{mutant}).[20] Each residue of α5- or α7-helices was mutated to other possible 19 natural amino acids. As a result, we found that some mutant variants showed better free binding energy than the wild-type (Figure 2A). Then, we selected the top four point mutations for each helix: A(101)R, N(109)M, N(109)K, and N(113)K of α5-helix (Figure 2B; hereinafter named **P1**), and T(139)R, F(140)R, T(141)F, and L(153)K of α7-helix (Figure 2C; hereinafter named **P2**). The wild type and mutant variants were then studied to determine their binding stability using steered molecular dynamics (SMD) at various pulling forces.[19] Consequently, **P1** variants were found to bind RHEB with more stability than **P2** variants, as suggested by the averaged root-mean square deviation values (Figures 2D,E, S1, and S2). These data were collected from 5000 points representing the displacement of the peptide variants from the initial binding site over the whole simulation time (10 ns). Therefore, most variants were significantly displaced from the initial poses at both pulling forces (0.025 or 0.25 Å/ns) with different binding stability for **P1** variants. These results alongside the calculated physical properties and predicted cell penetration probability provide strong evidence demonstrating the efficacy of **P1** for the intracellular targeting of RHEB (Figure 2F and Table S1).[22]

Owing to the small size of **P1** variants (13 aa) and the positive net charge derived from at least three arginine residues, enhanced CPP was observed over the negatively charged cell membrane (Figure 2F). Conversely, **P2** variants are rich in glutamic acid, which negatively charges the peptides and thus decreases their CPP (non-CPP) due to repulsion of the cell membrane (Figure 2F). Based on the findings of this computational analysis, we synthesized **P1_WT**, **P1_A(101)R**, **P1_N(109)M**, double mutants **P1_A(101)R_N(113)K**, **P2_WT**, and **P2_L(153)K**.

mTORC1 Kinase Assay. The synthetic peptides (purity 90−95%; Figures S3−S8) were then screened for mTORC1 inhibition through the phosphorylation inhibition of the downstream signals S6K1 and 4E-BP1.[19] Prestarved HeLa cells were treated with single doses (1 μM) of peptides or Torin1 (an ATP-competing inhibitor of mTOR) for 3 hours
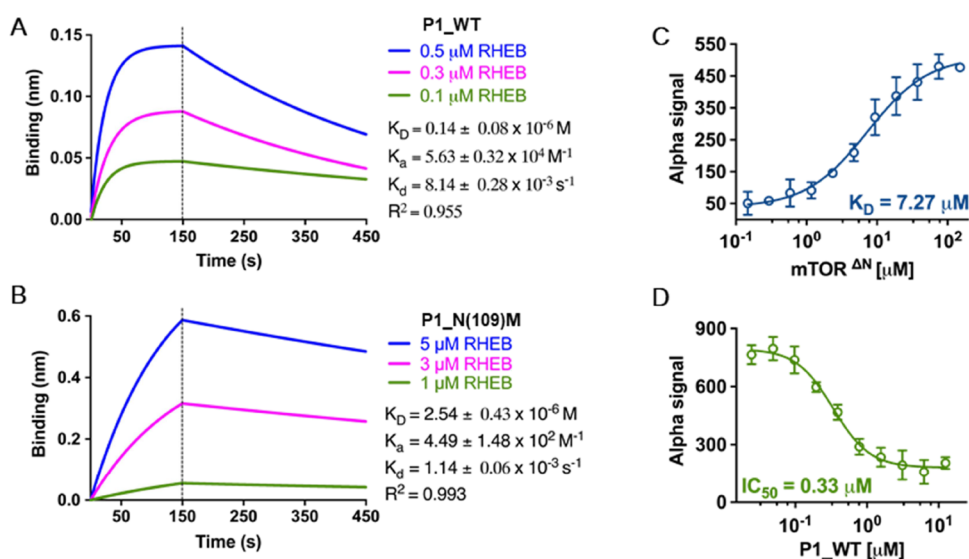
Figure 4. Binding kinetics of RHEB-targeting peptides. (A and B) Fitting curves of the BLI kinetics for **P1_WT** (A) and **P1_N(109)M** (B) with RHEB. Biotinylated peptides (100 nM) were immobilized onto streptavidin biosensors, and RHEB traces was used as analytes as indicated. Binding kinetics were calculated by the global fitting (1:1 binding) mode. K_D, the equilibrium dissociation constant; K_a, the association constant; K_d, the dissociation constant. The kinetics parameters are shown ± standard errors. See Figures S11 and S12 for BLI analysis views. (C) AlphaLISA binding of mTOR$^{\Delta N}$ domain with RHEB ($n = 3$). K_D value is shown. (D) Inhibition of mTOR$^{\Delta N}$-RHEB protein−protein interaction by the **P1_WT** peptide ($n = 3$). The half-maximal inhibitory concentration (IC$_{50}$) is shown.

and then induced with 100 nM of insulin for 30 min to stimulate mTORC1 activation by RHEB. As predicted, **P1** variants showed stronger inhibitory effects on mTORC1 activity than did **P2** variants (Figure 3A).

The arginine-rich sequence of **P1** variants potentially enhanced CPP and consequent mTORC1 inhibition, while **P2** variants did not. Unexpectedly, **P1_WT** inhibited mTORC1 activity more strongly than the mutant variants of **P1**. These results were confirmed by the dose-dependent elucidation of the inhibitory activity of **P1_WT** and **P1_N-(109)M** that showed a half-maximal inhibitory concentration (IC$_{50}$) of ∼0.3 μM and >10 μM for p-S6K1 and p-4E-BP1, respectively (Figure 3B,C). The stronger inhibitory effect of **P1_WT** suggests its efficiency to penetrate the cell membrane and bind with RHEB at higher affinity to inhibit mTORC1 activity.

Peptide Binding Kinetics. As previously reported, we prepared RHEB using the BL21(DE3) *E.coli* overexpression system.[12] Then, we measured the in vitro binding affinity (K_D) of **P1_WT** and **P1_N(109)M** with RHEB by using a bio-layer interferometry (BLI) system including streptavidin biosensors.[23] For that, we synthesized N-terminal-modified peptides with biotin by using NHS-(PEG)$_{24}$-biotin reagent (Figures S9 and S10). To measure the binding kinetics, the biotinylated peptides were immobilized onto the streptavidin biosensors and RHEB was used as analyte in a PBS buffer (pH 7.0) containing 0.02% tween-20. The results showed that **P1_WT** binds RHEB with higher affinity ($K_D = 0.14$ μM; Figures 4A and S11) than **P1_N(109)M** ($K_D = 2.54$ μM; Figures 4B and S12), which was associated with an inhibitory effect on mTORC1 activity.

Furthermore, we assayed the inhibitory effect of P1_WT for the PPI of RHEB-mTOR$^{\Delta N}$ using the AlphaLISA system (PerkinElmer, USA).[24] We used the 6xHis tagged RHEB (∼20 kDa) and mTOR$^{\Delta N}$ (∼13 kDa) prepared by the BL21(DE3) *E. coli* overexpression system.[12] RHEB was first de-tagged by thrombin and then labeled with biotin using a NHS-(PEG)$_{24}$-

biotin reagent. Biotinylated RHEB was mixed with different concentrations of 6xHis-mTOR$^{\Delta N}$ followed by the addition of streptavidin-coated donor beads and anti-6xHis-coated acceptor beads. The results showed that mTOR$^{\Delta N}$ bound with RHEB by a K_D value of 7.27 μM (Figure 4C), corresponding to the value reported by the BLI analysis ($K_D \sim 6.5$ μM).[12] Then, we evaluated the effect of **P1_WT** to inhibit RHEB-mTOR$^{\Delta N}$ interaction by preincubating RHEB with a series of different concentration of **P1_WT** before adding mTOR$^{\Delta N}$. As a result, **P1_WT** inhibited RHEB binding to mTOR$^{\Delta N}$ with an IC$_{50}$ value similar to that of mTORC1 activity inhibition (∼0.3 μM; Figures 3B−C and 4D).

■ CONCLUSIONS

A new modality of cancer therapy has been emerging by blocking PPIs involved in mTORC1 activation.[1] In this study, we aimed to inhibit mTORC1 by interfering with the RHEB-mTOR interaction on the lysosome. The large PPI area of RHEB-mTOR limits the efficacy of small molecules for inhibition. Instead, we employed small peptides to disturb the PPI based on the structural characteristics of the α5- and α7-helices of N-heat domain of mTOR, which directly interact with RHEB. Thus, we designed two different peptides, **P1** and **P2**, based on the sequences of α5- and α7-helices, respectively. We attempted to maturate the peptides via in silico point mutagenesis; however, the wild-type variant P1_WT remained the best binder during SMD simulations, corresponding with the wet experiments to confirm binding affinity. Previously, we successfully demonstrated that the in silico mutagenesis improved the immune checkpoint interaction of PD-1/PD-L1.[20] This suggests that in silico mutagenesis is more effective for proteins than peptides. In addition, the small size and positive net charge of **P1** variants were advantageous to higher cell-penetrating probability, while **P2** variants were not due to the negative net charge. This resulted in the improved inhibition of mTORC1 activity by **P1_WT** compared to that of the other selected variants because **P1_WT** bound with

RHEB at the sub-micromolar level, which corresponds to its inhibitory activity on RHEB-mTOR$^{\Delta N}$ interaction. Overall, this study is the first to demonstrate that the small peptide-based compound, **P1_WT**, inhibits the kinase activity of mTORC1 by disturbing the allosteric regulation of RHEB. P1_WT was designed based on the structural information involved in the mTORC1-RHEB binding. Similarly, we will be able to develop other peptide inhibitors based on PPI modes.

■ EXPERIMENTAL SECTION

Analysis of RHEB-mTORC1 Interaction. We used the cryo-EM structure of mTORC1 complexed with RHEB (PDB ID: 6BCU)[3] to analyze the RHEB-mTORC1 interaction by ICM-Pro 3.9 software (Molsoft L.L.C., USA).[21] We focused on the interaction of RHEB with the N-heat domain of mTOR (mTOR$^{\Delta N}$; aa 60−167). The α5-helix (aa 101−115) and α7-helix (aa 139−158) of mTOR$^{\Delta N}$ interact with switch II of RHEB (aa 63−79) to stabilize the PPI. Based on these interactions, we focused on the helical regions including amino acid sequence (101-ATRIGRFANYLRN-113) of α5-helix (hereinafter named **P1**) and (139-TFTAEYVEFEVKRA-LEWL-156) of α7-helix (hereinafter named **P2**).

In Silico Point-Mutagenesis of P1 and P2 Peptides. To screen and mature the binding affinities of the selected peptide sequences with RHEB, we applied the in silico point-mutagenesis approach to each residue independently. Each residue mutated to one of other 19 natural amino acids. We used the TryMutation mode of the ICM-Pro 3.9 software[20,21] to calculate the binding free energy ($\Delta\Delta G_{bind}$) for each mutated residue according to the following equation:

$$\Delta\Delta G_{bind} = \Delta G_{mutant} - \Delta G_{WT}$$

where the free binding energy was calculated by subtracting the wild-type free energy (ΔG_{WT}) from the point-mutant free energy (ΔG_{mutant}). The results indicated that lower binding free energy correlates with higher binding affinity.

SMD Simulations. We conducted SMD simulations to study the binding stability of the selected peptides with RHEB, as previously described.[19] For **P1** variants, we selected **P1_WT** (ATRIGRFANYLRN), **P1_A(101)R** (RTRIGRFANYLRN), **P1_N(109)M** (ATRIGRFAMYLRN), **P1_N(109)K** (AT-RIGRFAKYLRN), and **P1_N(113)K** (ATRIGRFANYLRK). For **P2** variants, we selected **P2_WT** (TFTAEYVEFEVKRA-LEWL), **P2_T(139)R** (RFTAEYVEFEVKRALEWL), **P2_F-(140)R** (TRTAEYVEFEVKRALEWL), **P2_T(141)F** (TFFAEYVEFEVKRALEWL), and **P2_L(153)K** (TFTAEY-VEFEVKRAKEWL). We used the super-computing system, SHIROKANE, of the Human Genome Center (HGC) at the University of Tokyo. We used the scalable molecular dynamics software NAMD-2.14 acerated with V100 GPU through the visual molecular dynamics interface.[25−27] This interface supported the QwikMD plugin to automatically generate a rectangular box buffered with 15 Å around macromolecules filled with 0.15 M NaCl and TIP3 water molecules in a CHARMM36 force field.[28−30] For the peptides, a stream force field (.str) was generated by the CGenFF server (https://cgenff.paramchem.org/).[31,32] For all SMD simulations, we set the spring constant of 7 kcal/mol/Å (1 kcal = 69.48 pN·Å). Two different pulling speeds, 0.025 and 0.25 Å/ns, were applied for 10 ns at 310 K and 1 atm, respectively. The pulling direction was set along with −Z.

Prediction of Cell-Penetrating Peptides (CPP). It is possible to predict and optimize cell penetration for peptides based on net charges. Therefore, we used the machine learning-based prediction of cell-penetrating peptides (MLCPP)[22] framework to evaluate the probability of the selected peptides entering the cell. MLCPP is an online platform (http://www.thegleelab.org/MLCPP/MLCPP.html) that employs machine learning models of two-layer prediction framework based on the calculated properties of the peptide sequence, considering amino acid sequence, atomic composition, and physiochemical properties. We entered the peptide sequences using the FASTA format in the field and submitted the job; the tabulated results appeared within a few minutes and indicated CPPs and non-CPPs.

Peptide Property Calculation. To analyze the physical properties of the selected peptides, we calculated the molecular weight (MW) and net charge (NetC) using the NovoPro peptide property calculator (https://www.novoprolabs.com/tools/calc_peptide_property) and the octanol/water partition coefficient (LogP) and aqueous solubility (LogS) using the ALOGPS 2.1 online program, which is provided by the Virtual Computational Chemistry Laboratory (VCCLAB) (http://www.vcclab.org /lab/alogps/).[33] We used the peptide sequences for calculations in NovoPro and used the SMILES format for calculations in ALOGPS 2.1.

Peptide Synthesis, Purification, and Analysis. Peptide synthesis, purification, and analysis were performed upon order at the RIKEN Research Resources Division (RRD; RIKEN, Wako, Japan).

a. *Synthesis.* To evaluate the inhibition activity of the peptides, we selected **P1_WT**, **P1_A(101)R**, **P1_N-(109)M**, **P1_A(101)R_N(113)K**, **P2_WT**, and **P2_L-(153)K** for synthesis. **P1_WT**, **P1_A(101)R**, **P1_A-(101)R_N(113)K**, **P2_WT**, and **P2_L(153)K** were automatically synthesized by MultiPep CF synthesizer (CEM Corporation, formerly INTAVIS Bioanalytical Instruments AG), while **P1_N(109)M** was synthesized by Liberty Blue synthesizer (CEM Corporation). For BLI binding kinetics, **P1_WT** and **P1_N(109)M** were labeled using NHS-(PEG)$_{24}$-biotin reagent at the N-terminal.

b. *Crude peptide analysis.* The crude peptides were analyzed using a high-performance liquid chromatography (HPLC) L-2000 system (Hitachi High-Tech Science Corporation, Japan) at 25 °C with Inertsil ODS-3 (250 × 4.6 mm I.D.) through a linear gradient mobile phase (1−51%) composed of 0.1% TFA in acetonitrile for 50 min.

c. *Peptide purification.* The peptides were purified by HPLC D-7000 (Hitachi High-Tech Science Corporation, Japan) at 25 °C using InertSustain C18 (250 × 20 mm I.D.).

d. *Pure peptide analysis.* The pure peptides were analyzed by HPLC Chromaster (Hitachi High-Tech Science Corporation, Japan) at 25 °C using InertSustain C18 (250 × 4.6 mm I.D.).

e. *Mass measurements.* The mass of the peptides was measured by the matrix-assisted laser desorption time-of-flight mass spectrometry (MALDI-TOF MS) using Microflex spectrometer (Bruker Daltonics, Germany).

mTORC1 Kinase Assay. To evaluate the inhibitory activity of the peptides on mTORC1 kinase activity, we used AlphaLISA SureFire Ultra HV p-S6K1 (T389) or p-4E-BP1 (T37/46) assay kits (PerkinElmer, USA) for detecting

mTORC1 phosphorylated products p-S6K or p-4E-BP1, respectively, as previously described.[19] Briefly, 10^4 HeLa cells/well were seeded in a 96-well plate in high-glucose D-MEM (FUJIFILM Wako Pure Chemicals Co., Japan) supplemented with 10% FBS and 1% P/S and were then incubated overnight (5% CO_2; 37 °C). The cells were starved in Opti-MEM reduced serum media (Thermo Fisher, USA) for 18 h and then treated with single dose (1 μM) or increasing concentrations of peptides for 3 h. After, cells were induced by 100 nM insulin for 30 min to enhance mTORC1 activation by RHEB. The cells were then lysed with 50 μL of 1× lysis buffer, which was freshly prepared by shaking for 10 min. Cell lysate (6 μL) was transferred to a 384-well OptiPlate (PerkinElmer, USA) and mixed with 3 μL of the Acceptor mix of anti-p(T389) S6K or anti-p(T37/46)4E-BP1. They were then top-sealed, covered, and incubated in the dark for 1 h at room temperature. Finally, 3 μL Donor mix of anti-S6K or anti-4E-BP1 was added under subdued light, followed by top sealing and incubation in the dark for >1 h at room temperature. The alpha signal was measured by the EnSpire plate reader (PerkinElmer, USA).

Protein Expression and Purification. In this study, we prepared RHEB (UniProt ID: Q15382) and mTOR$^{\Delta N}$ (UniProt ID: P42345), which were expressed and purified as previously described.[12] Briefly, RHEB or mTOR$^{\Delta N}$ genes were cloned into pET15b vector by In-Fusion cloning kit (Takara, Japan) and transformed into BL21(DE3) *E. coli* for protein expression. The 6xHis-tagged RHEB or mTOR$^{\Delta N}$ was then purified by Ni-NTA column (GE Healthcare, USA) and Superdex-200 column (GE Healthcare, USA), concentrated, and stored at −80 °C.[12]

BLI Binding Kinetics. We evaluated the binding kinetics of RHEB with **P1_WT** or **P1_N(109)M** peptides by the BLI method by using the BLItz instrument (FortéBio, USA) as previously described.[12,20] For this purpose, the peptides were N-terminally modified by NHS-(PEG)$_{24}$-biotin to immobilize them onto streptavidin biosensors. First, the biosensors (FortéBio, USA) were hydrated for 1 h in the kinetics buffer (PBS, pH 7.0 containing 0.02% (v/v) Tween-20). For the measurements, 100 nM biotinylated peptide in the kinetic buffer was immobilized onto the biosensors. The measurement cycle composed of 30 s initial baseline (kinetic buffer), 150 s peptide immobilization, 60 s baseline (kinetic buffer), 150 s RHEB association, and 300 s dissociation phases (kinetic buffer). A reference cycle was applied for each sensor by introducing RHEB only in the association phase to exclude nonspecific binding possibilities. RHEB concentrations were 0.1, 0.3, and 0.5 μM for **P1_WT** binding measurement and 1, 3, and 5 μM for **P1_N(109)M** binding measurement. All measurements were performed at 1000 rpm shaking speed at room temperature. Finally, we used BLItz Pro 1.2 software (FortéBio, USA) for curve fitting by using 1:1 binding kinetics.

RHEB de-Tagging and Biotinylation. We used our prepared tag-cut RHEB as previously described.[12] Briefly, 6xHis-RHEB was incubated with thrombin at a ratio of 1 mg protein: 10 units thrombin incubated overnight at room temperature on a rotator and purified by His SpinTrap column (GE Healthcare, USA) and HiTrap Benzamidine FF column (GE Healthcare, USA) to remove 6xHis tag and thrombin, respectively.

Tag-cut RHEB was then labeled with NHS-(PEG)$_{24}$-biotin using addition reaction of click chemistry as previously described to immobilize onto streptavidin-coated beads for AlphaLISA measurments.[20] Briefly, protein buffer was exchanged to PBS, pH 7.0 over 10 kDa MW-CO Amikon filter (Millipore (Merck), Germany). After protein concentration, RHEB was mixed with NHS-(PEG)$_{24}$-biotin at a 1:20 molar ratio in PBS and incubated at room temperature for 2 h. Finally, the mixture was washed with PBS over 10 kDa MW-CO Amikon filter several times to remove excess reagent, concentrated, and stored at −80 °C.

AlphaLISA Measurements. To evaluate the effect of **P1_WT** to inhibit RHEB-mTOR$^{\Delta N}$ interaction, we used the AlphaLISA-based assay as previously described.[12,20] First, we evaluated RHEB-mTOR$^{\Delta N}$ interaction by mixing different concentrations of 6xHis-mTOR$^{\Delta N}$ with 1 μM biotinylated RHEB in a 384-well OptiPlateTM (PerkinElmer, USA) followed by adding 100 μg/mL streptavidin-coated donor beads and 200 μg/mL anti-6xHis-coated acceptor beads. The plate was then sealed, covered, and incubated in the dark for >1 h at room temperature. The alpha signal was then measured by an EnSpire plate reader.

The effect of **P1_WT** on RHEB-mTOR$^{\Delta N}$ interaction was evaluated using the same method with some modifications. Increasing concentrations of **P1_WT** were incubated with 1 μM biotinylated RHEB; then, 1 μM of 6xHis-mTOR$^{\Delta N}$ was added followed by 100 μg/mL of streptavidin-coated donor beads and 200 μg/mL of anti-6xHis-coated acceptor beads. The plate was then sealed, covered, and incubated in the dark for >1 h at room temperature. The alpha signal was then measured by an EnSpire plate reader.

Data Analysis. Statistical significance and the number of samples are noted in figure legends where appropriate. Data are expressed as mean ± SD. Two-way ANOVA was used as indicated; **** for $P < 0.0001$ and ns for $P > 0.05$ with Tukey's test correction. Statistical analyses were performed using GraphPad Prism software v.9.3 (GraphPad, USA).

■ ASSOCIATED CONTENT

ⓈSupporting Information

The Supporting Information is available free of charge at https://pubs.acs.org/doi/10.1021/acsomega.2c01865.

SMD simulations, HPLC chromatograms, MALDI-MS spectra, and raw fitting view of BLI peptide binding kinetics (PDF)

Accession Codes

RHEB (UniProtKB ID: Q15382); mTOR (UniProtKB ID: P42345).

■ AUTHOR INFORMATION

Corresponding Author

Hideyuki Miyatake − *Department of Life Science, Graduate School of Science and Engineering, Saitama University, Saitama City, Saitama 338-8570, Japan; Nano Medical Engineering Laboratory, RIKEN Cluster for Pioneering Research, Wako, Saitama 351-0198, Japan;* ◉ orcid.org/0000-0001-8872-9784; Email: miyatake@riken.jp

Authors

Raef Shams − *Emergent Bioengineering Materials Research Team, RIKEN Center for Emergent Matter Science, Wako, Saitama 351-0198, Japan; Department of Life Science, Graduate School of Science and Engineering, Saitama University, Saitama City, Saitama 338-8570, Japan; Present Address: Biochemistry Division, Faculty of Science, Tanta*

University, Tanta 31527, Egypt (R.S.); ● orcid.org/0000-0003-4359-7030

Yoshihiro Ito − *Emergent Bioengineering Materials Research Team, RIKEN Center for Emergent Matter Science, Wako, Saitama 351-0198, Japan; Nano Medical Engineering Laboratory, RIKEN Cluster for Pioneering Research, Wako, Saitama 351-0198, Japan;* ● orcid.org/0000-0002-1154-253X

Complete contact information is available at:
https://pubs.acs.org/10.1021/acsomega.2c01865

Author Contributions

R.S. and H.M. conceived the study. Y.I. managed the research group. R.S. designed the peptides and conducted the experiments. H.M. conducted the SMD simulations. R.S. and H.M. wrote the manuscript. All authors checked and approved the experimental results and the manuscript.

Notes

The authors declare no competing financial interest.

■ ABBREVIATIONS

ATP, adenine triphosphate; AKT, protein kinase B; BLI, bio-layer interferometry; CPP, cell-penetrating peptides; Da, Dalton; DEP, disheveled-EGL-10-Pleackstrin domain; DEP-TOR, DEP domain-containing mTOR-interacting domain; 4E-BP1, eukaryotic translation initiation factor 4E-binding protein 1; GTP, guanidine triphosphate; IGF, insulin-like growth factor; mLST8, mammalian lethal with SEC13 protein 8; PI3K, phosphoinositide 3-kinases; PRAS40, 40 kDa proline-rich AKT substrate; PPI, protein−protein interaction; RAGs, RAS-related GTP-binding proteins; RAPTOR, regulatory-associated protein of mTOR; RHEB, Ras homolog enriched in brain; RMSD, root-mean square deviation; SBDD, structure-based drug design; S6K1, ribosomal protein S6 kinase 1; SMD, steered molecular dynamics; TSC, tuberous scleroses complex.

■ REFERENCES

(1) Shams, R.; Ito, Y.; Miyatake, H. Mapping of mTOR drug targets: Featured platforms for anti-cancer drug discovery. *Pharmacol. Ther.* **2022**, *232*, No. 108012.

(2) Liu, G. Y.; Sabatini, D. M. mTOR at the nexus of nutrition, growth, ageing and disease. *Nat. Rev. Mol. Cell Biol.* **2020**, *21*, 183−203.

(3) Yang, H.; Jiang, X.; Li, B.; Yang, H. J.; Miller, M.; Yang, A.; Dhar, A.; Pavletich, N. P. Mechanisms of mTORC1 activation by RHEB and inhibition by PRAS40. *Nature* **2017**, *552*, 368−373.

(4) Yang, H.; Rudge, D. G.; Koos, J. D.; Vaidialingam, B.; Yang, H. J.; Pavletich, N. P. mTOR kinase structure, mechanism and regulation. *Nature* **2013**, *497*, 217−223.

(5) Mossmann, D.; Park, S.; Hall, M. N. mTOR signalling and cellular metabolism are mutual determinants in cancer. *Nat. Rev. Cancer* **2018**, *18*, 744−757.

(6) Saxton, R. A.; Sabatini, D. M. mTOR Signaling in Growth, Metabolism, and Disease. *Cell* **2017**, *169*, 361−371.

(7) Rogala, K. B.; Gu, X.; Kedir, J. F.; Abu-Remaileh, M.; Bianchi, L. F.; Bottino, A. M. S.; Dueholm, R.; Niehaus, A.; Overwijn, D.; Fils, A. P.; Zhou, S. X.; Leary, D.; Laqtom, N. N.; Brignole, E. J.; Sabatini, D. M. Structural basis for the docking of mTORC1 on the lysosomal surface. *Science* **2019**, *366*, 468−475.

(8) Mahoney, S. J.; Narayan, S.; Molz, L.; Berstler, L. A.; Kang, S. A.; Vlasuk, G. P.; Saiah, E. A small molecule inhibitor of Rheb selectively targets mTORC1 signaling. *Nat. Commun.* **2018**, *9*, 548.

(9) Valvezan, A. J.; Manning, B. D. Molecular logic of mTORC1 signalling as a metabolic rheostat. *Nat. Metab.* **2019**, *1*, 321−333.

(10) Yonehara, R.; Nada, S.; Nakai, T.; Nakai, M.; Kitamura, A.; Ogawa, A.; Nakatsumi, H.; Nakayama, K. I.; Li, S.; Standley, D. M.; Yamashita, E.; Nakagawa, A.; Okada, M. Structural basis for the assembly of the Ragulator-Rag GTPase complex. *Nat. Commun.* **2017**, *8*, 1625.

(11) Anandapadamanaban, M.; Masson, G. R.; Perisic, O.; Berndt, A.; Kaufman, J.; Johnson, C. M.; Santhanam, B.; Rogala, K. B.; Sabatini, D. M.; Williams, R. L. Architecture of human Rag GTPase heterodimers and their complex with mTORC1. *Science* **2019**, *366*, 203−210.

(12) Shams, R.; Ito, Y.; Miyatake, H. Evaluation of the Binding Kinetics of RHEB with mTORC1 by In-Cell and In Vitro Assays. *Int. J. Mol. Sci.* **2021**, *22*, 8766.

(13) Long, X.; Lin, Y.; Ortiz-Vega, S.; Busch, S.; Avruch, J. The Rheb switch 2 segment is critical for signaling to target of rapamycin complex 1. *J. Biol. Chem.* **2007**, *282*, 18542−18551.

(14) Basso, A. D.; Mirza, A.; Liu, G.; Long, B. J.; Bishop, W. R.; Kirschmeier, P. The farnesyl transferase inhibitor (FTI) SCH66336 (lonafarnib) inhibits Rheb farnesylation and mTOR signaling. Role in FTI enhancement of taxane and tamoxifen anti-tumor activity. *J. Biol. Chem.* **2005**, *280*, 31101−31108.

(15) Ding, H.; McDonald, J. S.; Yun, S.; Schneider, P. A.; Peterson, K. L.; Flatten, K. S.; Loegering, D. A.; Oberg, A. L.; Riska, S. M.; Huang, S.; Sinicrope, F. A.; Adjei, A. A.; Karp, J. E.; Meng, X. W.; Kaufmann, S. H. Farnesyltransferase inhibitor tipifarnib inhibits Rheb prenylation and stabilizes Bax in acute myelogenous leukemia cells. *Haematologica* **2014**, *99*, 60−69.

(16) Baines, A. T.; Xu, D.; Der, C. J. Inhibition of Ras for cancer treatment: the search continues. *Future Med. Chem.* **2011**, *3*, 1787−1808.

(17) Wang, J.; Yao, X.; Huang, J. New tricks for human farnesyltransferase inhibitor: cancer and beyond. *MedChemComm* **2017**, *8*, 841−854.

(18) Ran, X.; Gestwicki, J. E. Inhibitors of protein-protein interactions (PPIs): an analysis of scaffold choices and buried surface area. *Curr. Opin. Chem. Biol.* **2018**, *44*, 75−86.

(19) Shams, R.; Matsukawa, A.; Ochi, Y.; Ito, Y.; Miyatake, H. In Silico and In Cell Hybrid Selection of Nonrapalog Ligands to Allosterically Inhibit the Kinase Activity of mTORC1. *J. Med. Chem.* **2022**, *65*, 1329−1341.

(20) Ning, B.; Ren, X.; Hagiwara, K.; Takeoka, S.; Ito, Y.; Miyatake, H. Development of a Non-IgG PD-1/PD-L1 Inhibitor by in Silico Mutagenesis and an In-Cell Protein-Protein Interaction Assay. *ACS Chem. Biol.* **2021**, *16*, 316−323.

(21) Abagyan, R.; Totrov, M.; Kuznetsov, D. ICM—A new method for protein modeling and design: Applications to docking and structure prediction from the distorted native conformation. *J. Comput. Chem.* **1994**, *15*, 488−506.

(22) Manavalan, B.; Subramaniyam, S.; Shin, T. H.; Kim, M. O.; Lee, G. Machine-Learning-Based Prediction of Cell-Penetrating Peptides and Their Uptake Efficiency with Improved Accuracy. *J. Proteome Res.* **2018**, *17*, 2715−2726.

(23) Touti, F.; Gates, Z. P.; Bandyopadhyay, A.; Lautrette, G.; Pentelute, B. L. In-solution enrichment identifies peptide inhibitors of protein-protein interactions. *Nat. Chem. Biol.* **2019**, *15*, 410−418.

(24) Yasgar, A.; Jadhav, A.; Simeonov, A.; Coussens, N. P. AlphaScreen-Based Assays: Ultra-High-Throughput Screening for Small-Molecule Inhibitors of Challenging Enzymes and Protein-Protein Interactions. *Methods Mol. Biol.* **2016**, *1439*, 77−98.

(25) Phillips, J. C.; Braun, R.; Wang, W.; Gumbart, J.; Tajkhorshid, E.; Villa, E.; Chipot, C.; Skeel, R. D.; Kale, L.; Schulten, K. Scalable Molecular Dynamics with NAMD. *J. Comput. Chem.* **2005**, *26*, 1781−1802.

(26) Phillips, J. C.; Hardy, D. J.; Maia, J. D. C.; Stone, J. E.; Ribeiro, J. V.; Bernardi, R. C.; Buch, R.; Fiorin, G.; Henin, J.; Jiang, W.; McGreevy, R.; Melo, M. C. R.; Radak, B. K.; Skeel, R. D.; Singharoy, A.; Wang, Y.; Roux, B.; Aksimentiev, A.; Luthey-Schulten, Z.; Kale, L. V.; Schulten, K.; Chipot, C.; Tajkhorshid, E. Scalable Molecular Dynamics on CPU and GPU Architectures with NAMD. *J. Chem. Phys.* **2020**, *153*, No. 044130.

(27) Humphrey, W.; Dalke, A.; Schulten, K. VMD: Visual Molecular Dynamics. *J. Mol. Graph* **1996**, *14*, 33−38.

(28) Ribeiro, J. V.; Bernardi, R. C.; Rudack, T.; Stone, J. E.; Phillips, J. C.; Freddolino, P. L.; Schulten, K. QwikMD - Integrative Molecular Dynamics Toolkit for Novices and Experts. *Sci. Rep.* **2016**, *6*, 26536.

(29) Jorgensen, W. L.; Chandrasekhar, J.; Madura, J. D.; Impey, R. W.; Klein, M. L. Comparison of Simple Potential Functions for Simulating Liquid Water. *J. Chem. Phys.* **1983**, *79*, 926−935.

(30) Huang, J.; MacKerell, A. D. CHARMM36 All-Atom Additive Protein Force Field: Validation Based on Comparison to NMR Data. *J. Comput. Chem.* **2013**, *34*, 2135−2145.

(31) Vanommeslaeghe, K.; MacKerell, A. D. Automation of the CHARMM General Force Field (CGenFF) I: Bond Perception and Atom Typing. *J. Chem. Inf. Model.* **2012**, *52*, 3144−3154.

(32) Vanommeslaeghe, K.; Raman, E. P.; MacKerell, A. D. Automation of the CHARMM General Force Field (CGenFF) II: Assignment of Bonded Parameters and Partial Atomic Charges. *J. Chem. Inf. Model.* **2012**, *52*, 3155−3168.

(33) Tetko, I. V.; Gasteiger, J.; Todeschini, R.; Mauri, A.; Livingstone, D.; Ertl, P.; Palyulin, V. A.; Radchenko, E. V.; Zefirov, N. S.; Makarenko, A. S.; Tanchuk, V. Y.; Prokopenko, V. V. Virtual computational chemistry laboratory–design and description. *J. Comput.-Aided Mol. Des.* **2005**, *19*, 453−463.